Toward data-driven resolvent analysis of nonlinear flows

By C. G. Hernández, K. Cao, B. Herrmann†, S. L. Brunton‡ AND B. J. McKeon

1. Motivation and objectives

The resolvent is a linear operator that governs how harmonic forcing inputs are amplified by the linear dynamics of a system and mapped onto harmonic response outputs. Resolvent analysis refers to the examination of this operator (a transfer function in the frequency domain) to find the most responsive inputs, their gains and the most receptive outputs. The analysis of this operator is related to the pseudospectrum of the linear operator, and its approximation of the dynamics of the full system is useful for modeling and controlling purposes. Trefethen *et al.* (1993) first introduced its use in the context of shear-driven flows, identifying the non-normality of the linearized operator as the cause of transient energy amplification of disturbances, even for cases where the eigenvalues were stable. McKeon, B. J. & Sharma, A. S. (2010) showed that resolvent analysis can be used to study the statistical structure of wall turbulence by interpreting the nonlinear term in the Fourier-transformed Navier–Stokes equations as an exogenous harmonic forcing.

Recently, Herrmann *et al.* (2021) proposed a method to perform resolvent analysis of linearly stable flows purely from time-resolved snapshot data. The method relies on Dynamic Mode Decomposition (DMD) (Schmid 2010) to approximate the eigenvalues and eigenfunctions of the system based on snapshots from one or more transient trajectories of the flow. They showed that, using an appropriate inner product, the resolvent of the matrix of DMD eigenvalues is the resolvent of the system projected onto the span of the DMD eigenvectors. These eigenvectors are then utilized to synthesize the resolvent modes in physical coordinates. Their algorithm was tested on data from the Ginzburg–Landau equation and transitional channel flow forced with various initial conditions to obtain the leading input and output resolvent modes and their associated gains without equations or data from adjoint simulations. This would enable resolvent analysis based also on experimental data.

Residual DMD (ResDMD) has recently been introduced in Colbrook *et al.* (2023) and is another method that can be utilized to obtain the eigenvalue-eigenvector pairs of a finite-dimension approximate Koopman operator and the residual values for how close they are compared to the true eigenvalue-eigenvector pairs of the underlying infinite-dimension Koopman operator (and thus the 'true dynamics') from the data snapshots of the system of interest. With certain formulations, the finite-dimension Koopman operator can be related directly to the DMD matrix used in the Data-Driven Resolvent Framework, and the residual values can be treated as uncertainty quantification for DMD. Eigenvalue-eigenvector pairs with significantly large residuals can be eliminated before constructing the projected resolvent operator.

† Department of Mechanical Engineering, Universidad de Chile
‡ Department of Mechanical Engineering, University of Washington

However, data-driven resolvent analysis relies on DMD, which can give a contaminated estimate of the linearized operator in the case of strong nonlinear effects. Generally, this is the case for turbulent flows, especially at high Reynolds numbers. Therefore, a new method was needed that is capable of separating the linear and nonlinear dynamics driving the evolution of spatiotemporal measurements of the system. By contrast, sparse identification methods learn the fully nonlinear models, disambiguating the linear and nonlinear effects, but they are restricted to low-dimensional systems. A recent method especially well suited to deal with these two issues is'Linear and Nonlinear Disambiguation Optimization' (LANDO) (Baddoo *et al.* 2022). LANDO performs kernel regression on a sparse dictionary of samples that contribute meaningfully to the dynamics, efficiently handling high-dimensional data, and is flexible enough to incorporate partial knowledge of system physics. Once the linear model contribution is obtained, the resulting operator evaluated on the data can be readily used for resolvent analysis.

In this brief, we combine all three methods, namely, data-driven resolvent analysis, ResDMD and LANDO to leverage data-driven resolvent analysis of nonlinear flows. The approach is tested on data from simulations of transitional channel flow and the Kuramoto-Sivashinsky (KS) equation on the attractor. Additionally, some preliminary results will be shown for turbulent channel flow in a minimal box unit. The remainder of the brief is organized as follows: A formulation of the data-driven resolvent analysis as well as ResDMD and LANDO methods are presented in Section 2. A description of the datasets employed in this work and preliminary results are provided in Section 3. Finally, our conclusions are offered in Section 4.

2. Formulation

Let us consider a forced linear dynamical system

$$\dot{\mathbf{x}} = \mathbf{A}\mathbf{x} + \mathbf{f}, \tag{2.1}$$

where $\mathbf{x} \in \mathbb{R}^n$ is the state vector, $\mathbf{A} \in \mathbb{C}^{n\times n}$ is the discretized linear operator, $\mathbf{f} \in \mathbb{C}^n$ is the external force and the dot denotes time differentiation. Now suppose $\mathbf{x}$ is the deviation from a stable steady state. For a harmonic $\mathbf{f}$ in the form $\mathbf{f}(t) = \hat{\mathbf{f}}e^{-i\omega t} + \text{c.c.}$, where c.c. means complex conjugate, $\omega \in \mathbb{R}$ is the angular driving frequency, and $t \in \mathbb{R}$ is the time variable. The long-term response is also harmonic $\mathbf{x}(t) = \widehat{\mathbf{x}}e^{-i\omega t} + \text{c.c.}$, with $\widehat{\mathbf{x}}$ governed by the particular solution to Eq. (2.1)

$$\widehat{\mathbf{x}} = (-i\omega\mathbf{I} - \mathbf{A})^{-1}\hat{\mathbf{f}} = \mathbf{H}(\omega)\hat{\mathbf{f}}, \tag{2.2}$$

where $\mathbf{I}$ is the $n \times n$ identity matrix and $\mathbf{H}(\omega)$ is the resolvent operator. We seek the largest input-output gain, optimized over all possible forcing vectors $\hat{\mathbf{f}}$

$$\sigma_1(\omega) = \max_{\hat{\mathbf{f}}\neq\mathbf{0}} \frac{\|\hat{\mathbf{x}}\|_{\mathbf{Q}}^2}{\|\hat{\mathbf{f}}\|_{\mathbf{Q}}^2} = \max_{\hat{\mathbf{f}}\neq\mathbf{0}} \frac{\|\mathbf{H}(\omega)\hat{\mathbf{f}}\|_{\mathbf{Q}}^2}{\|\hat{\mathbf{f}}\|_{\mathbf{Q}}^2}, \tag{2.3}$$

where $\|\widehat{\mathbf{x}}\|_{\mathbf{Q}}^2 = \widehat{\mathbf{x}}^*\mathbf{Q}\widehat{\mathbf{x}}$ measures the size of the state based on the metric given by the weighting matrix $\mathbf{Q}$, which accounts for the integration quadratures and nonuniform discretization. The asterisk denotes the conjugate transpose in this context. Using the Cholesky decomposition ($\mathbf{Q}$ is positive definite) to factorize $\mathbf{Q} = \mathbf{F}^*\mathbf{F}$, we obtain

$$\sigma_1(\omega) = \left\|\mathbf{F}\mathbf{H}(\omega)\mathbf{F}^{-1}\right\|_2^2. \tag{2.4}$$

The solution to Eq. (2.4) is then given by the singular value decomposition (SVD) of the weighted resolvent

$$\mathbf{F}\mathbf{H}(\omega)\mathbf{F}^{-1} = \mathbf{\Psi}_{\mathbf{F}}(\omega)\mathbf{\Sigma}(\omega)\mathbf{\Phi}_{\mathbf{F}}^{*}(\omega), \tag{2.5}$$

where $\mathbf{\Sigma} \in \mathbb{R}$ is a diagonal matrix containing the gains $\sigma_1 \geq \sigma_2 \geq \cdots \geq \sigma_n \geq 0$, and $\mathbf{\Phi}_{\mathbf{F}} = \mathbf{F}\left[\phi_1, \phi_2, \cdots, \phi_n\right]$ and $\mathbf{\Psi}_F = \mathbf{F}\left[\psi_1, \psi_2, \cdots, \psi_n\right]$ are unitary matrices whose columns, when left multiplied by $\mathbf{F}^{-1}$, are the input/output resolvent modes, respectively.

2.1. *Data-driven resolvent analysis*

Data-driven resolvent analysis (Herrmann *et al.* 2021) uses DMD to approximate the eigenvalues and eigenvectors of the dynamical system under study. In the absence of forcing, the evolution of measurements of Eq. (2.1) is given by

$$\mathbf{x}_{k+1} = \exp(\mathbf{A}\Delta t)\mathbf{x}_k, \tag{2.6}$$

where $\mathbf{x}_k$ is the measurement at time $t_k = k\Delta t$, with Δt the sampling time. In the 2-norm framework

$$\mathbf{F}\mathbf{x}_{k+1} = \mathbf{F}\exp(\mathbf{A}\Delta t)\mathbf{F}^{-1}\mathbf{F}\mathbf{x}_k = \mathbf{\Theta}\mathbf{F}\mathbf{x}_k, \tag{2.7}$$

where $\mathbf{\Theta} = \mathbf{F}\exp(\mathbf{A}\Delta t)\mathbf{F}^{-1}$ evolves the weighted measurements. Therefore, using the weighted measurements, we can proceed using DMD to approximate the linear operator. As outlined in Herrmann *et al.* (2021), the steps to perform data-driven resolvent analysis are listed below

1) The snapshots of the flow are collected as follows

$$\begin{aligned}
\mathbf{X} &= \mathbf{F}\left[\begin{array}{cccc|cccc|c|cccc} x_1^{(1)} & x_2^{(1)} & \cdots & x_m^{(1)} & x_1^{(2)} & x_2^{(2)} & \cdots & x_m^{(2)} & \cdots & x_1^{(p)} & x_2^{(p)} & \cdots & x_m^{(p)} \end{array}\right], \\
\mathbf{Y} &= \mathbf{F}\left[\begin{array}{cccc|cccc|c|cccc} x_2^{(1)} & x_3^{(1)} & \cdots & x_{m+1}^{(1)} & x_2^{(2)} & x_3^{(2)} & \cdots & x_{m+1}^{(2)} & \cdots & x_2^{(p)} & x_3^{(p)} & \cdots & x_{m+1}^{(p)} \end{array}\right],
\end{aligned} \tag{2.8}$$

where in the sample $x_k^{(j)}$, the subscript $k \in \{1, \cdots, m+1\}$ denotes the sample number, and the superscript $j \in \{1, \cdots, p\}$ denotes different trajectories starting from p initial conditions.

2) A rank-r truncated SVD of the snapshots is performed

$$\mathbf{X} = \mathbf{V}_{r,\mathbf{F}}\mathbf{D}_r\mathbf{W}_{r,\mathbf{F}}^{*}, \tag{2.9}$$

whose eigenvalues and eigenvectors are related to those of $\mathbf{A}$ via $\lambda_r = \log\left(\rho_j\right)/\Delta t$, $\mathbf{V}_r = \mathbf{F}^{-1}\mathbf{V}_{r,\mathbf{F}}$ and $\mathbf{W}_r = \mathbf{F}^{-1}\mathbf{W}_{r,\mathbf{F}}$ that satisfy

$$\mathbf{A}\mathbf{V} = \mathbf{V}\mathbf{\Lambda} \quad \text{and} \quad \mathbf{A}^{+}\mathbf{W} = \mathbf{W}\mathbf{\Lambda}^{*} \tag{2.10}$$

for an unknown operator $\mathbf{A}$, where $\mathbf{A}^{+} = \mathbf{Q}^{-1}\mathbf{A}^{*}\mathbf{Q}$ is its $\mathbf{Q}$-norm adjoint. The subscript r has been omitted. Here, DMD is used as a data-driven eigendecomposition.

3) We now seek an approximation of $\mathbf{H}(\omega)$ built on $\mathbf{\Lambda}_r$,$\mathbf{V}_r$, $\mathbf{W}_r$. We consider an eigenvector expansion of $\mathbf{x}$ and $\mathbf{f}$ as follows

$$\mathbf{x}(\mathbf{t}) = \mathbf{V}_r\mathbf{a}(t), \quad \mathbf{f}(\mathbf{t}) = \mathbf{V}_r\mathbf{b}(t), \tag{2.11}$$

where $\mathbf{a}, \mathbf{b}$ are the expansion coefficients in eigenvector coordinates. The projected system is then

$$\dot{\mathbf{a}} = \mathbf{\Lambda}_r\mathbf{a} + \mathbf{b}. \tag{2.12}$$

Because we are now working in different coordinates, if we want to retain the physical

meaning of the norm, we need to adjust our inner product accordingly, and the new weighting matrix is $\|\mathbf{x}\|_{\mathbf{Q}}^2 = \mathbf{x}^*\mathbf{Q}\mathbf{x} = \mathbf{a}^*\mathbf{V}_r^*\mathbf{Q}\mathbf{V}_r\mathbf{a} = \|\widetilde{\mathbf{F}}\mathbf{a}\|_2^2$, where we have defined $\widetilde{\mathbf{F}}$ from the Cholesky factorization of $\mathbf{V}_r^*\mathbf{Q}\mathbf{V}_r = \widetilde{\mathbf{F}}^*\widetilde{\mathbf{F}}$.
4) Resolvent analysis of $\dot{\mathbf{a}} = \mathbf{\Lambda}_r\mathbf{a} + \mathbf{b}$. The weighted resolvent modes and gains are obtained from the SVD of the projected resolvent as follows

$$\widetilde{\mathbf{F}}\left(-i\omega\mathbf{I} - \mathbf{\Lambda}_r\right)^{-1}\widetilde{\mathbf{F}}^{-1} = \mathbf{\Psi}_{\widetilde{\mathbf{F}}}(\omega)\mathbf{\Sigma}(\omega)\mathbf{\Phi}_{\widetilde{\mathbf{F}}}^*(\omega). \tag{2.13}$$

In physical coordinates, we can now recover the resolvent modes

$$\mathbf{\Phi} = \mathbf{V}_r\widetilde{\mathbf{F}}^{-1}\mathbf{\Phi}_{\widetilde{F}}^* \quad \text{and} \quad \mathbf{\Psi} = \mathbf{V}_r\widetilde{\mathbf{F}}^{-1}\mathbf{\Psi}_{\widetilde{F}}. \tag{2.14}$$

2.2. *ResDMD*

The method described by Colbrook *et al.* (2023) aims at obtaining the eigenvalue-eigenvector pairs of a finite-dimension approximate Koopman operator and the residual values for how close they are compared to the true eigenvalue-eigenvector pairs of the underlying infinite-dimension Koopman operator from the data snapshots of the system of interest. The algorithm is as follows:
1) Given a dictionary (set of basis functions) $\{\psi_1, \cdots, \psi_N\}$ of observables, DMD constructs a matrix $\mathbb{K} \in \mathbb{C}^{NxN}$ from the snapshot data $\left\{\mathbf{x}^{(m)}, \mathbf{y}^{(m)}\right\}_{m=1}^{M}$ that approximates $\mathcal{K}$ (the infinite-dimension Koopman operator) on the finite-dimension subspace $V_N = \text{span}\{\psi_1, \cdots, \psi_N\}$.
2) The solution to the optimization problem that minimizes the residual (error) obtained by the application of $\mathbb{K}$ to approximate the Koopman operator via a quadrature rule is

$$\mathbb{K} = \left(\psi_x^*\mathbf{W}\psi_x\right)^{\dagger}\left(\psi_x^*\mathbf{W}\psi_y\right) = \left(\sqrt{\mathbf{W}}\psi_x\right)^{\dagger}\sqrt{\mathbf{W}}\psi_y, \tag{2.15}$$

where $\mathbf{W}$ is the weighting matrix and $\psi_x, \psi_y \in \mathrm{C}^{M\times N}$.
3) The residual of the eigenvalue-eigenvector pair (λ, g) is approximated as follows

$$\text{res}(\lambda, g)^2 = \frac{g^*\left[\psi_y^*\mathbf{W}\psi_y - \lambda\left[\psi_x^*\mathbf{W}\psi_y\right]^* - \overline{\lambda}\psi_x^*\mathbf{W}\psi_y + |\lambda|^2\psi_x^*\mathbf{W}\psi_x\right]g}{g^*\left[\psi_x^*\mathbf{W}\psi_x\right]g} \tag{2.16}$$

for $\lambda \in \mathbb{C}$ and $g = \Psi\mathbf{g} \in V_N$, where g is the projection of a new observable onto the current dictionary of observables.
4) Now, we solve the eigenvalue problem $\left(\psi_x^*\mathbf{W}\psi_y\right)\mathbf{g} = \lambda\left(\psi_x^*\mathbf{W}\psi_x\right)\mathbf{g}$, and the residual $\text{res}(\lambda, g)$ is computed. Finally, the eigenvalues with $\text{res}(\lambda, g) > \varepsilon$ are discarded, with $\varepsilon > 0$ the goal accuracy.

2.3. *LANDO*

The method introduced in Baddoo *et al.* (2022) will be used here to separate the linear and nonlinear contributions. The steps of the algorithm are listed below.
1) The snapshots are collected as usual

$$\begin{aligned}\mathbf{X} &= \left[x_1^{(1)}x_2^{(1)}\cdots x_m^{(1)} \mid x_1^{(2)}x_2^{(2)}\cdots x_m^{(2)}\mid\cdots\mid x_1^{(p)}x_2^{(p)}\cdots x_m^{(p)}\right],\\ \mathbf{Y} &= \left[x_2^{(1)}x_3^{(1)}\cdots x_{m+1}^{(1)} \mid x_2^{(2)}x_3^{(2)}\cdots x_{m+1}^{(2)}\mid\cdots\mid x_2^{(p)}x_3^{(p)}\cdots x_{m+1}^{(p)}\right].\end{aligned} \tag{2.17}$$

2) Our optimization problem consists of finding a function $\mathbf{f}$ that suitably maps the training data. The function $\mathbf{f}$ is typically restricted to a given class of models (e.g.,

linear, polynomial, etc.), so that it may be written as the expansion

$$\mathbf{f} = \sum_{j=1}^{N} \xi_j \phi_j(x) \equiv \boldsymbol{\Xi}\phi(\mathbf{x}), \tag{2.18}$$

where $\mathbf{f}$ is our model, ϕ describes the feature library of N candidate terms and $\boldsymbol{\Xi}$ contains the coefficients that determine which model terms are active and to what degree. The optimization problem to be solved is

$$\underset{\boldsymbol{\Xi}}{\operatorname{argmin}} \|\mathbf{Y} - \boldsymbol{\Xi}\phi(\mathbf{X})\| + \alpha R(\boldsymbol{\Xi}), \tag{2.19}$$

where the second term $\alpha R(\boldsymbol{\Xi})$ is a regularizer. However, ϕ is generally large and the optimization problem becomes intractable, so we use an appropriate kernel function

$$\mathbf{f} = \sum_{j=1}^{m} w_j k\left(x_j, x\right) \equiv \mathbf{W}k(\mathbf{X}, x), \tag{2.20}$$

where the sum is over the number of snapshots (m) instead of the number of library elements (N). The optimization problem now becomes

$$\underset{W}{\operatorname{argmin}} \|\mathbf{Y} - \mathbf{W}k(\mathbf{X}, \mathbf{X})\| + \alpha R(\mathbf{W}). \tag{2.21}$$

3) An additional reduction to help handle large numbers of snapshots is the use of sparse dictionaries to learn kernel models, as follows

$$\mathbf{f} = \sum_{j=1}^{m} w_j k\left(x_j, x\right) \equiv \mathbf{W}k(\mathbf{X}, x) \approx \widetilde{\mathbf{W}}k(\widetilde{\mathbf{X}}, x), \tag{2.22}$$

where $\widetilde{\mathbf{X}}$ is the dictionary, and, the tilde means that the quantity is connected to it. The dictionary is constructed by considering each sample and determining whether it should be included in the dictionary. This is decided by checking if the sample can be approximated in the feature space using the current dictionary. This method is called the 'almost linearly dependent' (ALD) test: If a sample is almost linearly dependent on the current dictionary, then it is not added; otherwise, the dictionary must be updated with the current sample. Once the dictionary has been learned, the weights are calculated as

$$\widetilde{\mathbf{W}} = \mathbf{Y}k(\widetilde{\mathbf{X}}, x)^{\dagger}. \tag{2.23}$$

This kernel model is implicit, meaning that without further analysis we cannot interpret the model and understand the physical relationships that the model has learned.

3. Results

3.1. *Data sets*

Three data sets will be used to test our combined method: (1) transitional channel flow simulated in a small box $L_x/h = 2\pi$, $L_z/h = \pi$, with resolution $N_x = 32$, $N_y = 65$, $N_z = 32$, Reynolds number $Re = 2000$ and $N = 1000$ snapshots are considered, with $\Delta t = 0.5$, the initial condition is a localized impulse [computed with the spectral code CHANNELFLOW (Gibson *et al.* 2008)]; (2) KS equation on the chaotic attractor for $t_{final} = 15,000$ with $\Delta t = 1$ (computed with MATLAB's ODE45); and (3) turbulent channel flow simulated in a minimal box [using DIABLO (Bewley 2018)], $L_x/h = \pi$, $L_z/h = \pi/2$ with a

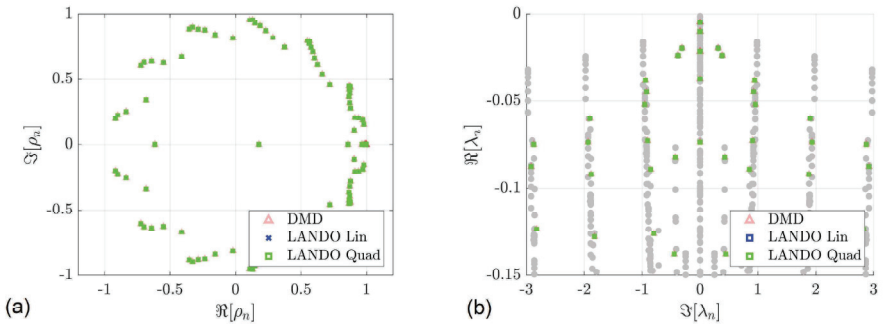

Figure 1: Eigenvalues D_r and Λ_r of the linear operator for the transitional channel flow case, regressed with LANDO (no dictionary) using linear and quadratic kernels. The number of POD modes retained is $r = 100$, onto which the snapshots have been projected. The operator-based eigenvalues are plotted in gray.

resolution $N_x = 64$, $N_y = 129$, $N_z = 64$ at Reynolds number $Re = 4348$ and $Re_\tau = 185$, with converged second-order statistics and $N = 500$ snapshots. The laminar profile has been subtracted in (1), and the mean flow has been subtracted from the data in (3).

3.2. *Transitional channel flow*

In this work, only a polynomial kernel of degree up to two will be considered, owing to the quadratic nature of the nonlinear terms in the Navier–Stokes equations. The kernel $k(x)$ has the form

$$k(x) = a + bx + cx^2, \tag{3.1}$$

where $a = 0$ and $b = 1$, $c = 0$ for the linear case, and $b = c = 1$ for the quadratic case. Another important point worth clarifying is that there is an equivalence between DMD and LANDO with a linear kernel as explained below.

1) DMD: The SVD of the snapshots is $X = U\Sigma V^*$; therefore, the DMD matrix is $\tilde{A} = U^*YV\Sigma^{-1}$.

2) LANDO with linear kernel: The kernel is constructed as $K = X^*X = V\Sigma^2V^*$. Now, the weights are $W = YK^\dagger = YV\Sigma^{-2}V^*$. Therefore, $\tilde{A} = U^*WV\Sigma = U^*YV\Sigma^{-2}V^*V\Sigma = U^*YV\Sigma^{-1}$, which is equivalent to the DMD matrix.

Figure 1 shows the eigenvalues of (a) the snapshots D_r and (b) the linear operator λ_r estimated with DMD and regressed with LANDO using linear and quadratic kernels. Here, 100 proper orthogonal decomposition (POD) modes have been retained and the operator has been projected onto them, with the aim of improving numerical accuracy given that the matrices resulting from the application of the algorithm in Section 2 often have very large condition numbers. For this first example, the effect of the dictionary has been eliminated by considering $\tilde{\mathbf{X}} = \mathbf{X}$; that is, we consider all snapshots in our dictionary. It can be observed that the eigenvalues agree extremely well: The markers for the DMD and LANDO linear cases sit behind those for the LANDO quadratic case. The operator-based eigenvalues are plotted in gray, showing a fair agreement as well. For the case under consideration (negligible nonlinear effects), LANDO with quadratic kernel is still able to give a great estimate of the linear operator.

Figure 2 shows the largest resolvent gain σ_1 as a function of ω for the three methods outlined above. The three match within 0.01%−1%. Figure 3 shows the **Q**-norm difference

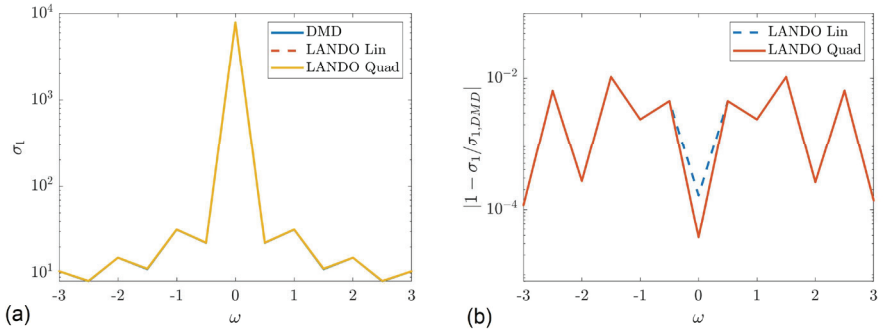

Figure 2: (a) Largest gain $\sigma_1(\omega)$ and (b) relative difference with respect to DMD $|1-\sigma_1(\omega)/\sigma_{1,DMD}(\omega)|$.

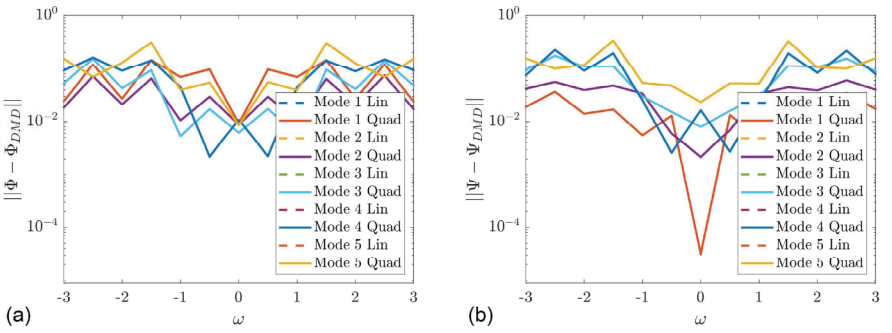

Figure 3: **Q**-norm difference of the resolvent modes regressed with LANDO Φ and Ψ with respect to DMD for various ω. The modes are orthonormal.

of the resolvent modes $\mathbf{\Phi}$ and $\mathbf{\Psi}$ from the linear operator regressed with LANDO with respect to those from DMD. The differences are in the range of $1\% - 30\%$ for $\mathbf{\Phi}$ and $0.01\% - 30\%$ for $\mathbf{\Psi}$. In effect, Figure 4 shows the first four forcing $\mathbf{\Phi_{1v}}$ and response $\mathbf{\Psi_{1u}}$ resolvent modes. It can be observed that they look very similar in the three cases compared.

Additionally, Figure 5 shows a color map of the residuals [Eq. (2.16)] of the eigenvalues calculated with DMD. The ResDMD algorithm, integrated with LANDO to leverage data-driven resolvent analysis of a turbulent flow, would discard the eigenvalues with larger residual, notably those in orange and yellow.

3.3. *KS equation*

The KS equation is a partial differential equation used to model a variety of (chaotic) physical phenomena like turbulence or chemical reactions. Here, we use data from a simulation of

$$u_t + u_{xxxx} + u_{xx} + \frac{1}{2}u_x^2 = 0, \tag{3.2}$$

on the attractor (transient removed) for $x \in [-L/2, L/2]$, with $L = 44.91$ and $t \in [0, 15,000]$ with $\Delta t = 1$, periodic boundary conditions and some given initial condition. The KS equation has some elements of the Navier–Stokes equations (nonlinearity, dif-

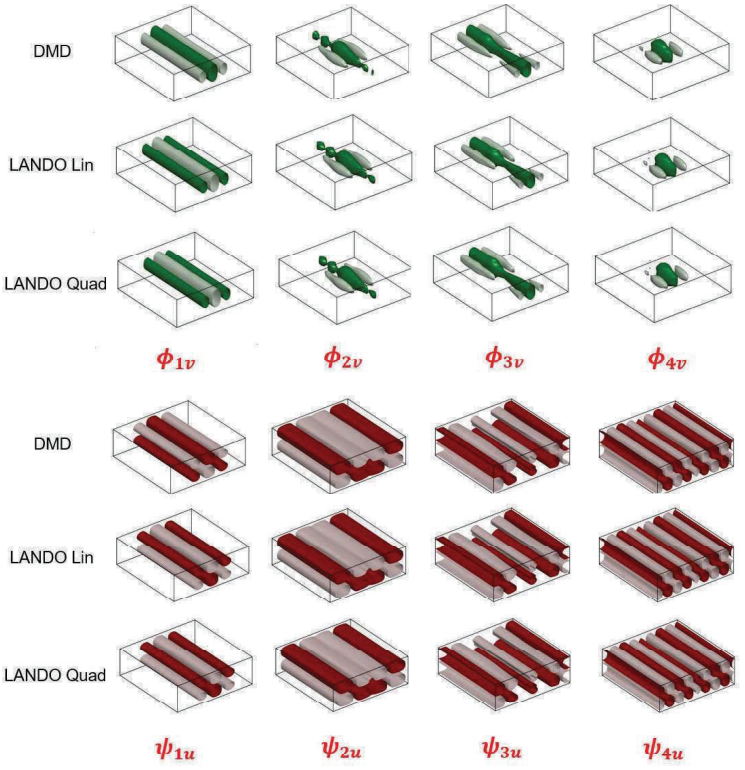

Figure 4: First four forcing $\mathbf{\Phi_{1v}}$ and response $\mathbf{\Psi_{1u}}$ resolvent modes using DMD and LANDO with linear and quadratic kernels.

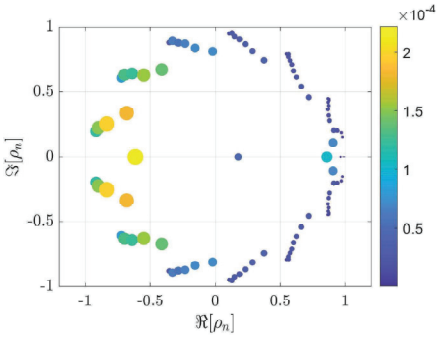

Figure 5: Residuals [Eq. (2.16)] of the eigenvalues calculated with ResDMD.

fusion, unsteadiness) and serves as an intermediate step to test our method after the transitional channel flow case (linear) and just before fully-nonlinear turbulent channel flow.

Figure 6 shows a comparison of the eigenvalues of Eq. (3.2): analytical $\lambda_n = (2n\pi/L)^2 - (2n\pi/L)^4$, and those obtained with DMD and LANDO. Clearly, LANDO outperforms DMD, obtaining regressed eigenvalues that match the analytical ones. This toy problem

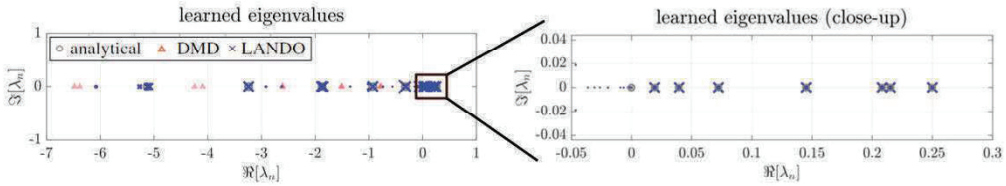

Figure 6: Eigenvalues of the linear operator of the KS equation: analytical, DMD and regressed with LANDO. The close-up shows a detailed view of the comparison. The size of the markers of the LANDO eigenvalues corresponds to the average projection of the training data onto the associated eigenvectors.

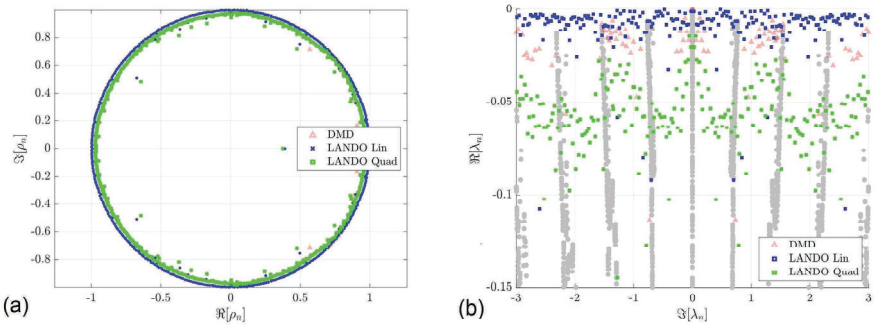

Figure 7: Eigenvalues D_r and Λ_r of the linear operator for the turbulent channel flow case, regressed with LANDO using linear and quadratic kernels. The number of POD modes retained is $r = 100$, and $N = 500$ snapshots are considered. The operator-based eigenvalues are plotted in gray.

is interesting because it shows that LANDO can regress eigenvalues of the linear operator of a nonlinear equation on the attractor, which is our case of interest in turbulent channel flow (sampling is done once the statistically steady state is achieved).

3.4. *Turbulent channel flow*

Now, our method is tested on time-resolved snapshot data from a numerical simulation of turbulent channel flow in a minimal box unit at $Re_\tau = 185$. The snapshots ($N = 500$) are taken once the statistically steady state is reached and the second-order statistics are converged.

Figure 7 shows the eigenvalues of the linear operator calculated with DMD and LANDO with a linear and quadratic kernels. The DMD eigenvalues lie near the real axis, as do the eigenvalues regressed by LANDO with linear kernel. Even though the results for LANDO with quadratic kernel are far from satisfactory when compared to the operator-based eigenvalues, we can see that the eigenvalues have larger real part, making the disambiguation slightly better than with the precedent methods.

4. Conclusions and future work

In this brief, we have investigated the data-driven resolvent analysis of several systems, ranging from almost-linear to fully-nonlinear turbulent channel flow. The methods em-

ployed, namely, data-driven resolvent analysis (Herrmann *et al.* 2021), LANDO (Baddoo *et al.* 2022) and ResDMD (Colbrook *et al.* 2023), have been shown to work well for a case with negligible nonlinearity, and LANDO clearly outperformed DMD for a simpler (although nonlinear) toy problem (KS equation). Preliminary results have shown that turbulent channel flow is a fairly more difficult problem, revealing an improvement in the regression of the linear operator but still far from the results given by operator-based resolvent analysis. More work is needed in this direction to understand the role of the coefficients of the kernel function [Eq. (3.1)] and other parameters like the size of the dictionary or the actual number of snapshots. Moreover, the robustness of the methods described here needs to be addressed in a comprehensive manner especially for the transitional channel flow case, where only a localized impulse initial condition has been verified. More work is needed to test other initial conditions like random or optimal disturbances. Finally, it is uncertain whether sampling one trajectory on the attractor is enough to regress the linear operator in turbulent channel flow or if the sampling must contain more departing trajectories on the attractor itself or in the transient phase. Future work will address these notable challenges.

Acknowledgments

This work is partly funded by NASA Transformational Tools and Techniques grant #80NSSC20M0201, and by the Department of Energy, National Nuclear Security Administration under Award Number DE-NA0003968 within the PSAAP III (INSIEME) Program at Stanford University.

REFERENCES

Baddoo, P. J., Herrmann, B., McKeon, B. J., & Brunton, S. L. 2022 Kernel learning for robust dynamic mode decomposition: Linear and nonlinear disambiguation optimization. *Proc. Royal Soc. A* **478**, 20210830.

Bewley, T. R. 2018 *Numerical Renaissance: Simulation, Optimisation and Control.* Renaissance Press.

Colbrook, M. J., Ayton, L. J., & Szőke, M. 2023 Residual dynamic mode decomposition: Robust and verified Koopmanism. *J. Fluid Mech.* **955**, A21.

Gibson, J. F., Halcrow, J., & Cvitanovic, P. 2008 Visualizing the geometry of state space in plane Couette flow. *J. Fluid Mech.* **611**, 107–130.

Herrmann, B., Baddoo, P. J., Semaan, R., Brunton, S. L., & McKeon, B. J. 2021 Data-driven resolvent analysis. *J. Fluid Mech.* **918**, A10.

McKeon, B. J. & Sharma, A. S. 2010 A critical-layer framework for turbulent pipe flow. *J. Fluid Mech.* **658**, 336–382.

Schmid, P. J. 2010 Dynamic mode decomposition of numerical and experimental data. *J. Fluid Mech.* **656**, 5–28.

Trefethen, L. N., Trefethen, A. E., Reddy, S. C., & Driscoll, T. A. 1993 Hydrodynamic stability without eigenvalues. *Science* **261**, 578–584.